Aust. J. Phys., 1983, **36**, 507–18

The Australian High Resolution Neutron Powder Diffractometer

C. J. Howard[A], *C. J. Ball*[A], *R. L. Davis*[B] *and M. M. Elcombe*[A]

[A] Australian Atomic Energy Commission Research Establishment,
Lucas Heights Research Laboratories, Private Mailbag, Sutherland, N.S.W. 2232.
[B] Australian Institute of Nuclear Science and Engineering,
Private Mailbag, Sutherland, N.S.W. 2232.

Abstract

The high resolution neutron powder diffractometer installed on the AAEC HIFAR reactor at Lucas Heights is described. The resolution is in good agreement with predictions and, although below the most optimistic estimates, the intensities are usable. Examples are given of problems solved using the diffractometer which could not have been solved either by X-ray diffraction or by use of a conventional neutron powder diffractometer. Plans for diffractometer development are outlined.

1. Introduction

Neutron diffraction techniques are widely used in studies of the structure of condensed matter. Information carried in the neutron diffraction pattern is often complementary to that obtained from X-ray diffraction since, in neutron scattering by nuclei, scattering lengths vary erratically with atomic number, whereas for X-rays scattered by atomic electrons, the scattering factors increase systematically with atomic number. Furthermore, neutron diffraction from magnetic materials provides information on magnetic structures unobtainable with conventional X-ray diffraction techniques.

The first neutron powder diffractometer was constructed by Wollan and Shull (1948) over thirty years ago, and neutron powder diffraction facilities have been available at the AAEC HIFAR reactor since 1961. The technique is used when samples are in polycrystalline (powder) form, in cases where it is too difficult to prepare single crystals of the size required for neutron investigation. Even when large single crystals are available, there can be a case for using powder specimens to reduce the effects of extinction on the results (Hewat 1974). For many years, applications were severely restricted by the resolution of available facilities. However, with the design (Hewat 1975), construction and demonstration (Hewat and Bailey 1976) of the high resolution diffractometer D1A at a guide tube position on the High Flux Reactor at the Institut Laue–Langevin, this restriction has been largely overcome. The development of D1A has undoubtedly contributed to the recent upsurge of interest in powder diffraction and its applications.

In this paper we describe the Australian High Resolution Powder Diffractometer (HRPD), installed at the HIFAR reactor and operational since June 1980. The HRPD has been constructed according to the design of Hewat (1975), and is the

0004-9506/83/040507$02.00

first such diffractometer to operate at (by current standards) a medium flux reactor. We report the performance of the HRPD in Sections 4 and 5 and a number of applications in Section 6. These applications are mostly to problems that have been difficult or impossible to solve using either neutron diffraction at conventional resolution or complementary techniques such as X-ray diffraction. Finally, plans for the further development of the HRPD are outlined in Section 7.

2. Diffractometer Resolution

The essential features of a two-axis powder diffractometer are a beam of thermal neutrons emerging from a reactor, a monochromator crystal which reflects neutrons of selected wavelength towards the sample, the sample itself, and a detector to count the neutrons scattered from the sample as a function of scattering angle 2θ. In the diffraction patterns obtained, the widths of the diffraction peaks vary with angle. According to Caglioti *et al.* (1958), the instrumental full width at half maximum (FWHM) B for a peak appearing at angle 2θ is given by

$$B^2 = U\tan^2\theta + V\tan\theta + W, \tag{1}$$

where U, V, W are constants for a given experimental arrangement. The take-off angle $2\theta_M$ from the monochromator is a critical parameter, since the constants U and V depend upon it, and the peak width B is at a minimum near the parallel focusing position $2\theta = 2\theta_M$. Also, the width of the band of wavelengths selected by the monochromator is proportional to $\cot\theta_M$. A diffractometer with a relatively high take-off angle will make use of a narrower band of neutron wavelengths, so that the available intensity will be less but the resolution will be generally better.

Most neutron powder diffractometers are built with take-off angles in the range 30°–60° and they give good intensity, but the resolution in the diffraction pattern deteriorates for $2\theta > 2\theta_M$. Hewat (1975) pointed out that in a typical diffraction pattern the separation of the peaks is expected to be a minimum at $2\theta \approx 90°$, and that it is desirable for a diffractometer to have good resolution in this vicinity. Hewat compared the resolution derived from equation (1) with expected peak separations across the pattern and concluded that the best overall match would result from a design with $2\theta_M \approx 120°$. Hewat and Bailey (1976) implemented such a design in D1A with $2\theta_M = 122°$ and obtained impressive results.

3. Description of HRPD

In Fig. 1 we show a simplified diagram of the HRPD; more detailed information is given in Table 1. As shown, the external fixed shielding is constructed to provide a take-off angle of 120°. The diffractometer is, however, not restricted to the high resolution mode, as there is an alternative position for the monochromator nearer to the reactor where the take-off angle is 45°. Location of the monochromator at this position allows operation as a more conventional, higher intensity, lower resolution diffractometer. Another feature is the facility for removing and replacing the primary beam collimator, presently a Soller collimator which limits the horizontal divergence of the primary beam to 0·20°. By replacing this collimator, the divergence of the primary beam can be varied to an upper limit on horizontal divergence of 0·45°.

At the 120° take-off position, the monochromator is located 6·77 m from the reactor tank. Placing the monochromator nearer the reactor face would have meant higher intensities and less shielding; however, the choice was dictated by the location of adjacent facilities. A total of 30 t ($=3\times10^4$ kg) of external fixed shielding is required because of the long neutron flight path and the location of the HRPD at the reactor face. It is in the shielding that the HRPD differs most noticeably from the D1A, which is located in a beam hall remote from the reactor face where shielding requirements are minimal.

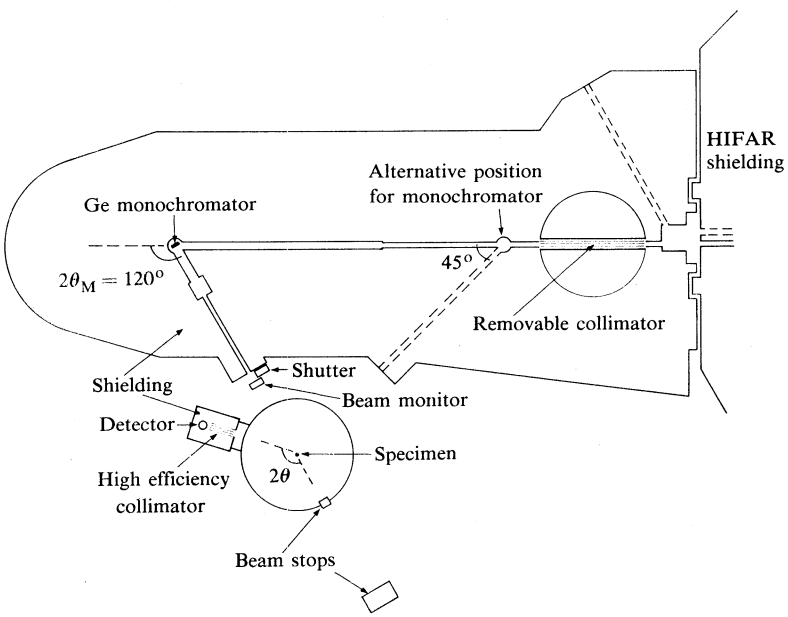

Fig. 1. Schematic diagram of the diffractometer. Neutrons from the reactor HIFAR are first collimated, then impinge upon the monochromator which reflects neutrons of the desired wavelength onto the specimen. The diffraction pattern (scattered intensity against scattering angle) is recorded by the detector as it moves around the specimen. For further details, see Section 3 and Table 1.

The monochromator is a germanium crystal mounted with the [$\bar{1}$10] direction vertical, so that rotation of the monochromator around this axis brings successive (*hhl*) planes into the reflecting position. As is common practice, we employ reflections from odd index planes in the expectation of obtaining beams free from $\lambda/2$ contamination; nevertheless, we have encountered one case of $\lambda/2$ contamination (see Section 4).

Neutrons scattered from the specimen are registered by a ^{3}He detector, mounted on an arm which can be driven around the specimen. In front of the detector is a high efficiency 'Rutherford Laboratory' Soller collimator. During normal operation, the detector counts at a fixed position for as long as it takes a neutron beam monitor to register a preset number of counts; the count recorded by the detector and the angle (from a SONY Rotary Magnescale Model MSE-6480) are then printed and punched on tape, and then the detector arm is driven by a stepping motor to the next position.

Table 1. Details of HRPD

Neutron source	HIFAR reactor with thermal neutron flux $\approx 1{\cdot}3 \times 10^{18}\,m^{-2}\,s^{-1}$. Neutrons enter a collimator set into HIFAR shielding through an 'obround' window 38 mm wide by 51 mm high
Neutron source to monochromator	Neutrons emerge from collimator in HIFAR shielding and pass through removable collimator located in external shielding (see Section 3)
Monochromator	Located to provide take-off angle of 120°. Alternative position available where take-off angle is 45°. Monochromator is 'squashed' crystal of germanium 75 mm in diam. and 10 mm thick. Mosaic spread is nominally 0·20°. Flat face is (335) plane and crystal is mounted with [$\bar{1}$10] vertically upward. (Note that cross product of vectors in directions of primary and reflected beams is also vertically upwards)
Monochromator to specimen	Neutrons pass through removable flight tube with aperture 16 mm wide by 51 mm high. Tube controls beam size at specimen position. At end of tube is low efficiency fission chamber used as neutron beam monitor
Specimen	Held in thin-walled aluminium or vanadium cylindrical container 12–16 mm diam. and 50 mm high. Specimen is rotated about vertical axis to reduce effects of preferred orientation. Furnaces and cryostats for specimen can be supported
Specimen to neutron detector	In front of detector is high efficiency 'Rutherford Laboratory' Soller collimator with aperture 20 mm wide by 100 mm high (see Hewat and Bailey 1976)
Neutron detector	25 mm diam. ^{3}He detector filled to 405 kPa. Detector (and collimator) are rotated around specimen. Accessible range of 2θ is $-40°$ to 160° and usual step size is 0·05°
Distances and angles	

Leg	Distance (m)	Horiz. div.[A] (deg.)	Vert. div.[A] (deg.)
Neutron source to monochromator	6·77	0·20[B,C]	0·51
Monochromator to specimen	1·82	0·62[C,D]	1·18[D]
Specimen to neutron detector	0·66	0·17[E]	5·03[D]

Mass of shielding	Mass of fixed shielding $\approx$30 tonne, counter shielding $\approx$30 kg

[A] Divergences are defined in accordance with Caglioti *et al.* (1958) and Hewat (1975).
[B] Value normally controlled by removable collimator.
[C] A lower value is appropriate when monochromator is set with its face nearly parallel to this leg of neutron flight path.
[D] Influenced by dimensions of specimen. Value calculated for a cylindrical specimen 13·5 mm diam. by 16 mm high.
[E] Controlled by high efficiency collimator.

4. Diffractometer Performance

The diffractometer has operated successfully at a number of wavelengths. At each wavelength, the beam has been photographed, the neutron flux at the specimen position measured by the activation of gold foils, and the diffraction pattern from a standard powder specimen of α-alumina recorded. The standard powder specimen is a cylinder of mass 8·87 g, diameter 13·5 mm and height 15·8 mm, which was prepared for an International Union of Crystallography intercomparison project (Andresen and Sabine 1977). Fig. 2*a* shows a typical diffraction pattern from the standard specimen at the neutron wavelength λ = 1·376 Å, and the results at this and other wavelengths are summarized in Table 2.

The excellent resolution of the diffractometer can be seen in Fig. 2. The variation of peak width across the pattern is much the same at each wavelength, the only exception being at low angles where the peaks in the patterns at other wavelengths are up to 20% wider. The variation of peak width has been determined from equation (1), with values of U, V, W calculated from theory (Caglioti *et al.* 1958; see also Hewat 1975) using the diffractometer parameters of Table 1. As shown in Fig. 2*b*, there is good agreement between observed and calculated peak widths.

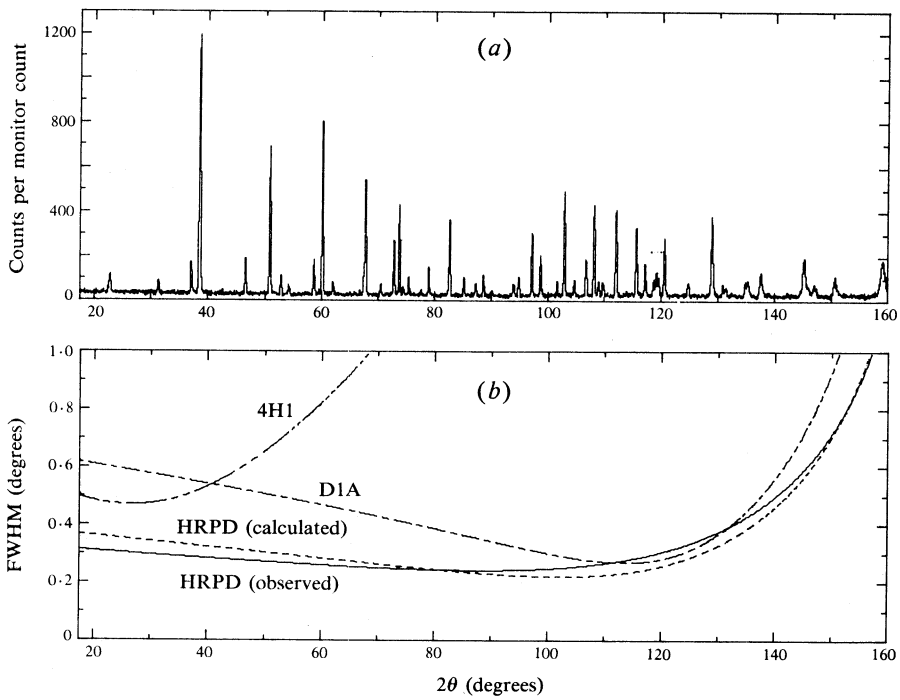

Fig. 2. In (*a*) we show the diffraction pattern from the alumina standard specimen recorded by the HRPD at $\lambda = 1{\cdot}376$ Å. The variation of peak width across this pattern is displayed in (*b*), together with the variation calculated from data in Table 1. Included for comparison are the peak widths for the high resolution diffractometer D1A at the Institut Laue–Langevin and the conventional Australian diffractometer 4H1.

Table 2 includes data on neutron fluxes and peak count rates at different wavelengths. Neutron fluxes were measured by gold foil activation techniques (Andresen and Sabine 1977). The measured flux of $1{\cdot}32 \times 10^{12}$ m^{-2}s^{-1} at the monochromator position agrees with the calculated value. However, at the specimen position, the measured values are more difficult to explain. At 1·500 Å, for example, the ratio of the flux at the specimen position to the (polychromatic) flux at the monochromator is $2{\cdot}5 \times 10^{-4}$, so the monochromator reflectivity defined by Sabine and Weinstock (1969) is $4{\cdot}0 \times 10^{-4}$. From Bragg's law, if the angles of incidence across the monochromator vary over a range $\Delta\theta_M$, then the reflected wavelengths cover a range

$$\Delta\lambda = \lambda \cot\theta_M \Delta\theta_M . \qquad (2)$$

Taking $\Delta\theta_M = 0{\cdot}2°$ (based on the source to monochromator divergence alone), we find that $\Delta\lambda = 3\times10^{-3}$ Å. If all the neutrons in this wavelength range were reflected, the reflectivity of the monochromator would be $1{\cdot}8\times10^{-3}$. Thus, there is evidence that the utilization of neutrons of the desired wavelength and direction is only about 20%. It has been established that a small gain could be achieved, with little deterioration in resolution, by opening out the flight tube to allow a greater horizontal divergence between monochromator and specimen. In addition, investigation of the monochromator crystal, with a view to its possible replacement, would be worth while.

Table 2. Performance of diffractometer at several wavelengths

Plane[A]	λ[B] (Å)	Contamination[C]	Flux at specimen[D] ($m^{-2}s^{-1}$)	Diffraction pattern from alumina specimen[E]: Count rate at peak of (113) reflection (s^{-1})	Peak/background at (113) reflection
(337)	1·202		$2{\cdot}4(4)\times10^8$	5·8	26
(117)	1·376		$3{\cdot}9(2)\times10^8$	9·3	41
(335)	1·500		$3{\cdot}3(5)\times10^8$	14·2	55
(115)	1·893		$4{\cdot}2(4)\times10^8$	18·9	88
(331)	2·256	16%$\lambda/2$, 7%$\lambda/3$	$1{\cdot}8(1)\times10^8$	11·9	73

[A] Monochromator plane in reflecting position. The (335) plane is parallel to crystal face, so (335) is a symmetric reflection. Other reflections are asymmetric. The (337), (117) and (115) concentrate the beam, while (331) broadens it. By remounting the monochromator so that $[1\bar{1}0]$ is upward, (331) could be obtained in a concentrating configuration with resulting gain in flux.

[B] Neutron wavelength is derived from diffraction pattern from alumina standard, assuming $a = 4{\cdot}758$ Å and $c = 12{\cdot}991$ Å.

[C] From examination of diffraction pattern for alumina standard (see Section 4). Percentages represent ratio of flux at contaminant wavelength to flux at wavelength tabulated.

[D] Neutron flux at specimen position. Flux measured at monochromator position was $1{\cdot}32\times10^{12}$ $m^{-2}s^{-1}$, using activation of gold foils. Value for $\lambda = 2{\cdot}256$ Å has been corrected to exclude contaminants.

[E] In all patterns peak widths are adequately described by equation (1) with $U = 0{\cdot}058$, $V = -0{\cdot}114$ and $W = 0{\cdot}122$.

The wavelengths in Table 2 are derived from the diffraction patterns from the standard alumina specimen and are accurate and reproducible to $\approx0{\cdot}001$ Å. These wavelengths are consistent with those expected from a germanium crystal ($a = 5{\cdot}6576$ Å) at a take-off angle of 120·7°. Examination of the diffraction patterns from the standard alumina specimen showed no sign of contaminants, except at $\lambda = 2{\cdot}256$ Å where $\lambda/2$ and $\lambda/3$ contaminants produced (113) peaks with intensities which were, after correction for background, 5% and 1% respectively of the intensity of the 2·256 Å (113) reflection. Taking into account the wavelength dependence of the detector efficiency and the dependence of reflecting power on wavelength and angle, we estimate the fluxes of the $\lambda/2$ and $\lambda/3$ contaminants in the beam to be 16% and 7% of the flux at 2·256 Å respectively. The $\lambda/2$ contamination is attributed to successive reflections from the $(\bar{1}1\bar{1})$ and (753) planes, or equally from reflections from the $(1\bar{1}\bar{1})$ and (573) planes. The experience serves as a warning that beams obtained from odd index germanium reflections are not always free from $\lambda/2$ contamination.

Finally, we remark that the peak-to-background ratios in Table 2 are significantly influenced by neutron background in the reactor sealed building, with only a small proportion of this background being attributable to leakage from the HRPD shielding. This background gives a contribution of $\approx 0 \cdot 13$ counts s^{-1}, which could be reduced by improving the detector shielding (and this will be done when the detector modifications described in Section 7 are completed).

5. Analysis of Diffraction Patterns from Alumina

In the testing of the diffractometer we collected comprehensive data from the standard alumina specimen, comprising complete diffraction patterns recorded as far as 160° in 2θ at five different wavelengths. Each diffraction pattern has been analysed by the Rietveld (1969) method, using a local version of a computer program by Wiles and Young (1981) in which the diffraction peaks were assumed to be basically gaussian, a sum of five gaussians being used to allow for peak asymmetry (Howard 1982). The weighting used was simply that given by $(w_i)^{-1} = y_i$. The background, calculated from the function

$$y_b = B_{-1}(2\theta)^{-1} + B_0 + B_1(2\theta) + B_2(2\theta)^2 , \tag{3}$$

was refined. The $(2\theta)^{-1}$ term was added to account for the observed increase in background below about 15° in 2θ, an increase which could not be satisfactorily described with only the positive powers of 2θ supplied by Wiles and Young. Sixteen parameters were refined: the zero point, the scale, the two lattice parameters, the atomic position parameters (two to be determined), the two isotropic thermal parameters, the three peak width parameters which appear in equation (1), the peak asymmetry parameter, and the four background parameters given in equation (3). In the 2·256 Å case, the pattern resulting from the $\lambda/2$ contaminant was included in the analysis. A summary of the results is given in Table 3 for the six specimen parameters, with certain measures of the goodness of fit (Wiles and Young 1981); note that lower values of the goodness of fit indicators correspond to better fits of the calculated to the recorded pattern.

The parameters listed in Table 3 can be compared with those obtained at other facilities. Hewat and Bailey (1976), using D1A, recorded a pattern with an alumina specimen from the same batch used here and analysed it by the Rietveld method. More recently, Jorgensen and Rotella (1982) reported results obtained with other specimens from the same batch using the high resolution time-of-flight powder diffractometer at the Argonne ZING-P′ pulsed neutron source. The results from these two studies and the present work are collected in Table 4 and show excellent agreement.

It is interesting to examine how the parameters in Table 3 vary with wavelength as it has been suggested (Sabine 1982) that powder data may be affected by such phenomena as absorption, extinction and multiple scattering. Neglect of these effects would then lead to systematic errors in the parameters, and a monotonic variation of (refined) parameters with wavelength might be expected. In the present case, there is no apparent monotonic variation of parameters with wavelength, however they still may be affected by systematic errors which depend in a less obvious way (or not at all) on wavelength. Despite this possibility, and also the criticism

Table 3. Parameters for alumina determined from neutron diffraction patterns by profile refinement method

λ[A] (Å)	Value of specimen parameters as determined in refinement[B]						Goodness of fit indicators[C]			
	a (Å)	c (Å)	z(Al)	x(O)	B(Al) (Å^2)	B(O) (Å^2)	R_p (%)	R_{wp} (%)	R_{wp}[D] (%)	R_B (%)
1·202	4·7605(1)	12·9997(3)	0·3522(1)	0·3064(2)	0·25(2)	0·31(2)	9·59	12·70	11·85	2·67
1·376	4·7563(1)	12·9891(3)	0·3521(2)	0·3063(2)	0·18(3)	0·20(2)	10·64	14·78	14·13	2·20
1·500	4·7574(1)	12·9920(3)	0·3525(1)	0·3066(2)	0·12(3)	0·23(2)	10·78	15·47	13·65	2·08
1·893	4·7575(1)	12·9926(4)	0·3522(1)	0·3059(2)	0·22(5)	0·25(4)	9·56	14·00	12·60	0·89
2·256	4·7579(1)	12·9935(4)	0·3521(3)	0·3059(3)	0·25(11)	0·31(7)	12·01	17·16	15·84	1·42

[A] Profile refinement programs are not generally capable of refining neutron wavelength. Accordingly, λ is set at (nominal) value shown and lattice parameters refined.
[B] For Al_2O_3, space group is $R\bar{3}c$ (No. 167), hexagonal axes being used, with $b_{Al} = 3{\cdot}449$ fm and $b_O = 5{\cdot}803$ fm.
[C] For definition of goodness of fit indicators see Wiles and Young (1981).
[D] Expected value.

Table 4. Parameters for alumina determined from neutron powder diffraction using different facilities

Location	Facility	Details	Values of specimen parameters determined by profile refinement[A]					
			a (Å)	c/a	z(Al)	x(O)	B(Al) (Å^2)	B(O) (Å^2)
Institut Laue–Langevin, Grenoble	D1A	$\lambda = 1{\cdot}38$ Å[B]	4·763	2·73095(6)	0·35222(7)	0·30635(8)	0·24	0·22
Argonne National Laboratory, Argonne	HRPD	Time-of-flight at $2\theta = 160°$[C]	4·763	2·73095(6)	0·35222(5)	0·30642(5)	0·155	0·187
AAEC Research Establishment, Sydney	HRPD	Weighted mean of entries in Table 3	4·758	2·73091(6)	0·35228(5)	0·30626(9)	0·20(1)	0·25(1)

[A] Cell parameters from Grenoble and Argonne were derived from values quoted for rhombohedral cell. Equivalent isotropic thermal parameters were derived from anisotropic parameters from Grenoble and Argonne (see Willis and Pryor 1975). Since correlations between different anisotropic thermal parameters are unpublished, no proper estimates can be made of errors in equivalent isotropic parameters.
[B] Hewat and Bailey (1976). [C] Jorgensen and Rotella (1982).

by Sakata and Cooper (1979) and Cooper (1982) of the reliability of the estimated standard deviations provided by the Rietveld method, we find that the scatter of results in Table 3 does not greatly exceed that expected on the basis of the estimated standard deviations obtained from the Rietveld analysis. [For further discussion of the work of Sakata and Cooper (1979), see Prince (1981), Hewat and Sabine (1981) and Scott (1983).]

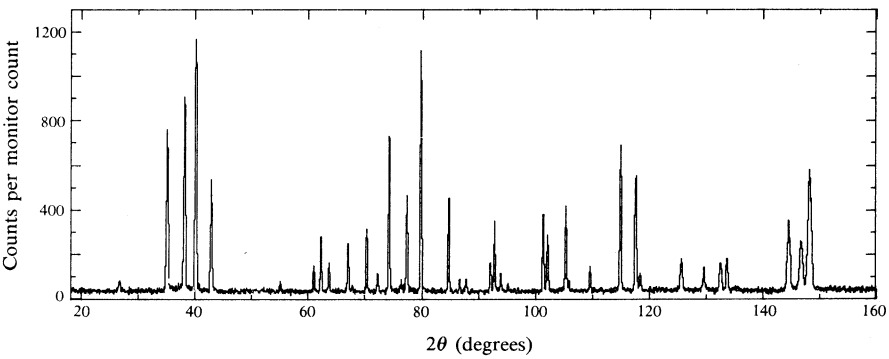

Fig. 3. Diffraction pattern from TiO_2 recorded using the HRPD at $\lambda = 1{\cdot}500$ Å. Analysis of this pattern by the Rietveld method yields a precise value for the parameter describing the position of the oxygen nucleus.

6. Applications

There is a large class of problems in which the use of neutron powder diffraction is appropriate. In many applications—such as those which involve the study of magnetic ordering, the location of hydrogen in metallic hydrides, or structures in which iron must be distinguished from cobalt (or silicon from aluminium)—the problems are either very difficult or intractable without neutron techniques. In other applications, neutron techniques provide information complementary to that obtained with X-rays or, for example, in the study of samples in furnaces, the transparency to neutrons of convenient structural materials is an advantage. Applications of these techniques were restricted until the construction of the high resolution facilities D1A at the Institut Laue–Langevin (Hewat and Bailey 1976), HRPD at Argonne (Jorgensen and Rotella 1982) and HRPD at Lucas Heights. The improved resolution means that measurements on simple structures can be made with greater precision, and structures previously too complex for study by neutron powder diffraction now fall within the scope of the technique. At present, the low data acquisition rates are the major limitation of the Australian HRPD; for example, the pattern in Fig. 2*a* was recorded at a 2θ scan rate of $1{\cdot}4°\ h^{-1}$. Further improvements are expected to increase data acquisition rates eight-fold (see Section 7).

The HRPD is relatively easy to operate, and techniques for analysis of neutron powder diffraction patterns, such as the Rietveld method, are already well developed (see e.g. Cheetham and Taylor 1977). The operation of the HRPD is in fact no more difficult than that of an X-ray powder diffractometer, the major difference from the experimentalist's point of view being the considerably larger sample required, and the resolution in the diffraction pattern is no longer markedly inferior to that in the corresponding X-ray pattern.

Some applications of the HRPD to date are as follows.

Rutile

The HRPD has been used in an investigation (Sabine and Howard 1982) of rutile, TiO_2, to test a suggestion that the oxygen ion is polarized to such a degree that the centroid of the electronic charge distribution, as determined by X-ray diffraction, might be significantly displaced from the nucleus. The position of the oxygen nucleus was determined from the neutron diffraction pattern (see Fig. 3) by the Rietveld method. The result agreed very closely with the position determined in previous X-ray studies, and there was certainly no discrepancy of the magnitude suggested. Neutrons were essential to this investigation since it was the nuclear position that was to be determined; high resolution was required to determine this position with adequate precision.

α-UF_5/U_2F_9

The pattern from an α-UF_5/U_2F_9 mixture has been analysed (Howard *et al.* 1982) to obtain the atomic position and isotropic thermal parameters for both α-UF_5 and U_2F_9. Neutrons were used because it is difficult to establish fluorine positions from X-ray data dominated by scattering from the heavy element. The mixture was produced by heating a sample of β-UF_5 at 180°C until there was no further change in the diffraction pattern. The mixtures were first prepared at Lucas Heights and the neutron diffraction pattern recorded in 1970 and in 1974; however, the resolution was such that at neither attempt could the mixture be identified. In the present attempt using the HRPD, the pattern was recorded, peak positions were determined using standard curve fitting procedures, corrections were applied for the vertical divergence effect (by adding $\frac{1}{3}P\cot 2\theta$ with $P = 0{\cdot}155$), and then the peaks were indexed. This led to a successful identification of the mixture. A comparison of the observed angles in the α-UF_5 diffraction pattern with those calculated showed that the positions of well resolved diffraction peaks had been measured to an accuracy approaching $0{\cdot}01°$.

Lead Dioxides

The HRPD has been used to study the crystal structures of chemically and electrolytically prepared varieties of α-PbO_2 and β-PbO_2 (Hill 1982), which are the primary constituents of the positive plate in a charged lead/acid battery. Once again the neutron technique produced useful results where scattering from heavy elements would have made X-ray studies very difficult.

Fergusonite

As a final example, we report a current investigation of the mineral fergusonite (W. W. Barker, personal communication). This naturally occurring mineral is usually 'metamict' (see Graham 1974), but occasionally it is found in tetragonal form. After heating to $\approx$1000°C and then cooling, a monoclinic form is produced. The monoclinic form transforms reversibly to a tetragonal form at $\approx$830°C. This phase transition is being studied in synthetic fergusonite, $YNbO_4$, using neutron diffraction to determine the crystal structure of the high temperature tetragonal phase, and to examine the slight shifts in the oxygen position in the change to the monoclinic structure. Here neutrons offer suitable scattering lengths and the advantage of convenient high temperature operation. A preliminary analysis of the results suggests

that the structure of the high temperature tetragonal phase is not identical to that of the naturally occurring tetragonal form, nor do the oxygen shifts conform with earlier expectations.

7. Future Development of HRPD

As indicated earlier, improvements to increase the data acquisition rate will soon be implemented. Following Hewat and Bailey (1976), we will replace the single detector, with its Soller collimator, by an array of detectors, each with a Soller collimator. The detector arm is to carry eight detectors (with collimators) mounted at 2θ intervals of 6° so that, as the detector arm is moved around the sample, eight diffraction patterns will be recorded simultaneously. A computer will be attached to compare and combine the patterns from the eight detectors, leading to a substantial increase in the data acquisition rate.

Improvements can also be made in the sample environment. At present, most samples are studied in air at room temperature and pressure. For low temperature studies, a top-loading liquid helium cryostat is available, the tails in this cryostat being constructed from vanadium, chosen for its neutron scattering properties. High temperatures up to ≈ 1200°C can be achieved in the simple furnace described by Bailey and Bennett (1979). Developments to provide high pressures, atmospheres of selected gases, higher temperatures, improved temperature control etc. will proceed as the demand arises.

8. Summary

A high resolution neutron powder diffractometer based on the Hewat (1975) design has been constructed and installed at the HIFAR reactor. The resolution is excellent, and when improvements in the rate of data acquisition are completed, the diffractometer will be comparable with the advanced facilities at Grenoble (D1A) and Argonne (HRPD). The diffractometer is relatively easy to operate and programs for data analysis are available. Since there are numerous instances in which neutron techniques offer a significant advantage over X-rays, many applications are foreseen.

Acknowledgments

Many people have contributed to the establishment of the diffractometer described. Special thanks are due to Professor T. M. Sabine and Dr J. C. Taylor whose powers of persuasion did much to get the project under way, to Mr P. T. Sirkka who supervised the construction of the main shield, and to Messrs C. P. Bock, D. K. McEachern, R. A. Phillips and K. Pickup who have provided first class technical assistance at call. The authors are grateful for assistance from the Physics and Materials Workshop of the New South Wales Institute of Technology in the construction of the monochromator mount. Finally, the authors wish to thank Dr A. W. Hewat for the interest he has shown in the project and for his expert advice.

References

Andresen, A. F., and Sabine, T. M. (1977). *J. Appl. Crystallogr.* **10**, 497–501.
Bailey, F. P., and Bennett, C. E. G. (1979). *J. Appl. Crystallogr.* **12**, 403–4.
Caglioti, G., Paoletti, A., and Ricci, F. P. (1958). *Nucl. Instrum. Methods* **3**, 223–8.
Cheetham, A. K., and Taylor, J. C. (1977). *J. Solid State Chem.* **1**, 253–75.

Cooper, M. J. (1982). *Acta Crystallogr.* A **38**, 264–9.
Graham, J. (1974). *Proc. R. Aust. Chem. Inst.* **41**, 62–4.
Hewat, A. W. (1974). 'Diffraction Studies of Real Atoms and Real Crystals', pp. 86–7 (Australian Academy of Science: Canberra).
Hewat, A. W. (1975). *Nucl. Instrum. Methods* **127**, 361–79.
Hewat, A. W., and Bailey, I. (1976). *Nucl. Instrum. Methods* **137**, 463–71.
Hewat, A. W., and Sabine, T. M. (1981). *Aust. J. Phys.* **34**, 707–12.
Hill, R. J. (1982). *Mater. Res. Bull.* **17**, 769–84.
Howard, C. J. (1982). *J. Appl. Crystallogr.* **15**, 615–20.
Howard, C. J., Taylor, J. C., and Waugh, A. B. (1982). *J. Solid State Chem.* **45**, 396–8.
Jorgensen, J. D., and Rotella, F. J. (1982). *J. Appl. Crystallogr.* **15**, 27–34.
Prince, E. (1981). *J. Appl. Crystallogr.* **14**, 157–9.
Rietveld, H. M. (1969). *J. Appl. Crystallogr.* **2**, 65–71.
Sabine, T. M. (1982). NSWIT Int. Rep. Nos PMR 13, 14, 15.
Sabine, T. M., and Howard, C. J. (1982). *Acta Crystallogr.* B **38**, 701–2.
Sabine, T. M., and Weinstock, E. V. (1969). *J. Appl. Crystallogr.* **2**, 141–2.
Sakata, M., and Cooper, M. J. (1979). *J. Appl. Crystallogr.* **12**, 554–63.
Scott, H. G. (1983). *J. Appl. Crystallogr.* **16**, 159–63.
Wiles, D. B., and Young, R. A. (1981). *J. Appl. Crystallogr.* **14**, 149–51.
Willis, B. T. M., and Pryor, A. W. (1975). 'Thermal Vibrations in Crystallography', p. 102 (Cambridge Univ. Press).
Wollan, E. O., and Shull, C. G. (1948). *Phys. Rev.* **73**, 830–41.

Manuscript received 18 November 1982, accepted 17 March 1983